ICAS 2020 SHANG HAI
32nd Congress of the International Council of the Aeronautical Sciences
September 6-10, 2021
Pudong Shangri-La, Shanghai, China

Design Optimization of Airfoils at Ultra-Low Reynolds Numbers

Jianhua Xu, Dan Li, Wenping Song*, Zhonghua Han & Huijing Li

National Key Laboratory of Science and Technology on Aerodynamic Design and Research, School of Aeronautics, Northwestern Polytechnical University, Xi'an 710072, China

Abstract

Spoon shaped airfoil has high lift-to-drag ratio at ultra-low Reynolds numbers (ranges from 10,000 to 100,000), but instable separated flow on lower surface near trailing edge result to obvious unsteady effect, which affects the controllability and stability of the aircraft. This paper aims to design airfoils not only to improve the time-averaged lift-to-drag ratio, but also to weaken the unsteady effect. An efficient optimizer based on Kriging surrogate model, named "SurroOpt" is used for airfoil design. An in-house URANS (unsteady Reynolds-averaged Navier-Stokes) solver with SST transition model for flow transition is utilized to simulate the flows around airfoils. Both single-point and two-point design are investigated. The results demonstrate that the time-averaged lift-to-drag ratio of the optimized airfoil is higher than that of baseline in a wide range of angles of attack. Meanwhile, the unsteady amplitudes of aerodynamic force are reduced. It is concluded that the developed unsteady aerodynamic design method achieves the design goal of improving lift-to-drag ratio and reducing unsteady effect.

Keywords: ultra-low Reynolds numbers, laminar separation bubble, unsteady aerodynamic design of airfoil

1. Introduction

The propeller propulsion system is the only feasible power system of the aircraft in near-space. At the altitude of 25 km, the density of the atmosphere is only about 3% of the density of the ground. Such low air density results to the low Reynolds numbers ranging from 10,000 to 100,000, named ultra-low Reynolds numbers in this paper.

The flow around airfoils at this ultra-low Reynolds numbers behave more complex, such as unsteady laminar separation bubbles. Meanwhile, the lift-to-drag ratio decreases dramatically, even to less than 30. This results in a significant reduction in propeller efficiency, which affects the cruise time and wind resistance of airships and UAVs.

In 2010, Srinath et al.[1][2] first found that a special shape like a "spoon" has higher lift-to-drag ratio in laminar flow, at the Reynolds number of 10,000. Then, Zhang et al.[3] studied and analyzed the spoon shaped airfoil, and designed a spoon shaped airfoil at the Reynolds number of 10,000~100,000. Their study shown that the lift-to-drag ratio of spoon shaped airfoil, at Reynolds number less than 150,000, is significantly higher than SD8040, a conventional low Reynolds number airfoil. In addition, compared with conventional airfoils, the lift-to-drag ratio of the spoon shaped airfoil does not change significantly with Reynolds number.

All of the above studies are based on laminar flow hypothesis. However, the experimental results show that laminar separation and flow transition still exist on airfoils with Reynolds number less than 100,000[4]. In addition, they only take into account the time-averaged aerodynamic characteristics. Although the time-averaged lift-to-drag ratio is obviously improved, the unsteady amplitude caused by laminar separation bubble may be larger, which is also undesirable.

This paper aims to develop an unsteady aerodynamic design method at ultra-low Reynolds numbers. The objective is not only to improve the lift-to-drag ratio, but also to weaken the unsteady effect. The remainder of this paper is organized as follows. In section 2, the in-house URANS solver "PMNS2D" coupled with SST transition model for flow transition are introduced and validated. In section3, the problems of the spoon shaped airfoil is proposed. Section 4 describes the method for unsteady design of airfoil. Section 5 demonstrates the design results and discussion. The last section is for the conclusions.

2. URANS Solver and its Validation

"PMNS2D" is an in-house RANS solver for two-dimensional flow simulation. It can be used to calculate the steady and unsteady aerodynamic forces of airfoils. This solver is based on the cell-centered finite volume method[5], with Jameson's central scheme for spatial discretization and implicit Lower-Upper Symmetric Gauss-Seidel[6] scheme for time stepping. The two-equation SST k-ω model[7] is used to turbulence closure with γ-$Re_{\theta t}$ model[8] for transition prediction (Transition SST).

Eppler 387 airfoil is used to validate the solver. Figure 1 shows the grid of airfoil, with a size of 545×185. Where, 385 points on the airfoil, and the distance between wall and far-field is 30c. First, steady flows are simulated under the condition of Ma = 0.09 and Re = 300,000. Figure 2 shows that the results of transition SST have better agreement with experimental data than that of full turbulent simulation.

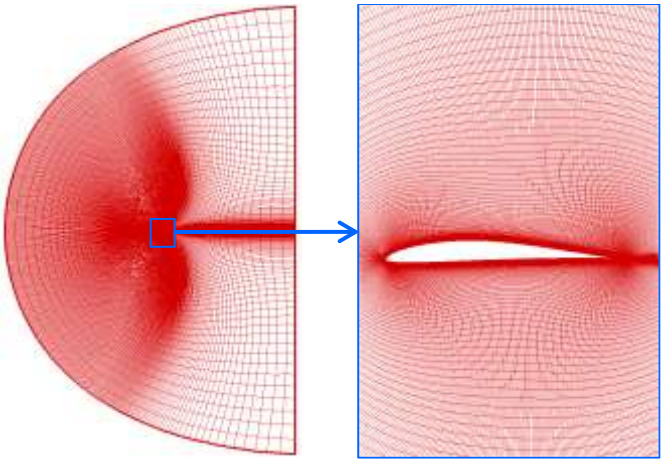

Figure 1 Grid of Eppler 387 airfoil

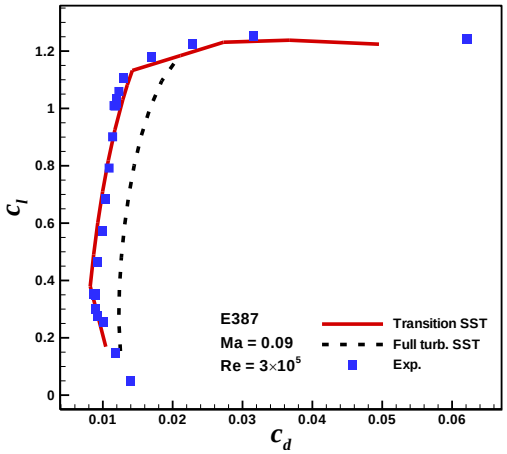

Figure 2 Comparison of c_d-c_l between PMNS2D and experimental data

Then, unsteady flows are simulated under the condition of Ma = 0.09, Re = 300,000 and α=0°. For this case, three different physical time steps are used, $dt_1=\pi c/V_\infty/200$, $dt_2=\pi c/V_\infty/500$ and $dt_3=\pi c/V_\infty/1000$. The periodicity of aerodynamic force is different with different physical time step, as shown in Figure 3. The main reason is that the structure of unsteady laminar separation bubble captured varies with physical time step, as shown in Figure 4. However, Figure 5 shows that the time-averaged pressure distributions by different physical time steps are all agree well with the experimental data, as well as the steady results. In addition, the pressure distribution with the minimum time step is closer to the experimental value, especially near the separation bubble. Table 1 shows that the experimental values of aerodynamic force are all in the range of unsteady calculation.

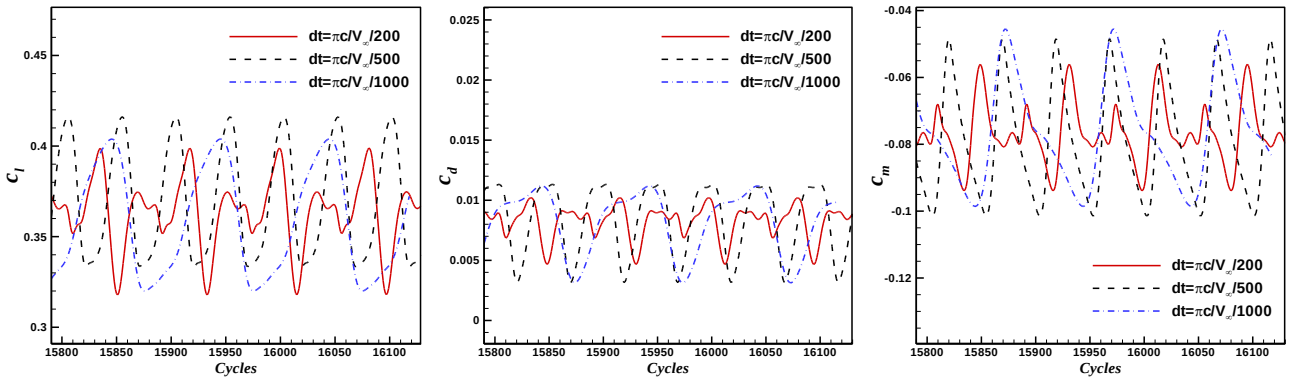

Figure 3 Periodic aerodynamic forces for different physical time steps

(a) $dt_1=\pi c/V_\infty/200$

(b) $dt_2=\pi c/V_\infty/500$

(c) $dt_3=\pi c/V_\infty/1000$

Figure 4 Periodic structure of unsteady laminar separation bubble varies with physical time step

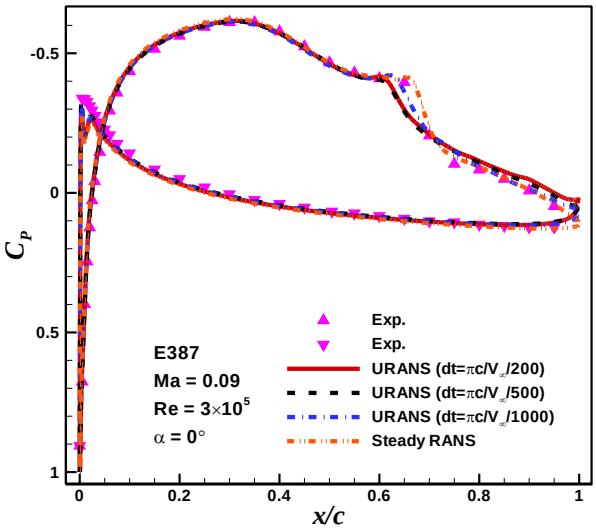

Figure 5 Pressure distributions by unsteady and steady calculations agree well with experimental data

Table 1 Comparison of steady, unsteady and experimental aerodynamic force

	Exp.	Unsteady ($dt_1=\pi c/V_\infty/200$)	Unsteady ($dt_1=\pi c/V_\infty/500$)	Unsteady ($dt_1=\pi c/V_\infty/1000$)
Lift coefficient	0.352	0.3178~0.3989	0.3334~0.4160	0.3200~0.4039
Drag coefficient	0.0089	0.004668~0.01020	0.003163~0.01132	0.003134~0.01119
Moment coefficient	-0.0768	-0.09389~-0.05606	-0.1014~-0.04844	-0.09857~-0.04552

3. Problems of Spoon Shaped Airfoil

Aerodynamic performance of a conventional airfoil Eppler 387 (E387) and a spoon shaped airfoil SPLRM (Figure 6) are compared at Ma = 0.3 and c_l = 0.8.Figure 7 gives the lift-to-drag ratio and the amplitude of unsteady force. The conventional airfoil Eppler 387 has higher time-averaged lift-to-drag ratio at Reynolds number larger than 50,000, and the spoon shaped airfoil SPLRM has higher time-averaged lift-to-drag ratio at Reynolds number lower than 50,000. SPLRM has a lift-to-drag ratio 34% higher than E387 at a Reynolds number of 30,000, and 55% higher than E387 at a Reynolds number of 20,000. In addition, the amplitude of SPLRM is larger than that of E387. This shows that although the spoon shaped airfoil can significantly improve the time-averaged lift-to-drag ratio, the unsteady characteristics may be more obvious, as shown in Figure 8 and Figure 9.

Figure 10 and Figure 11 shows the unsteady laminar separation bubble of E387 and SPLRM airfoils at cl = 0.8, respectively. The laminar separation bubbles on the upper surface of E387 are significantly larger than that of SPLRM. Larger separation bubbles mean that the thickness of the equivalent shape outside the boundary layer is larger, which leads to an increase in pressure drag. This is the reason why the lift-to-drag ratio of conventional airfoils is smaller than that of spoon shaped airfoils at ultra-low Reynolds number. Although the separation bubbles of E387 are relatively large, they are stable, so there is no significant unsteady aerodynamic characteristics. However, also there exist separation region on the lower surface near the trailing edge for the spoon shaped airfoil. The strong instability of this separation is the main reason for the unsteady aerodynamic force of the spoon shaped airfoil.

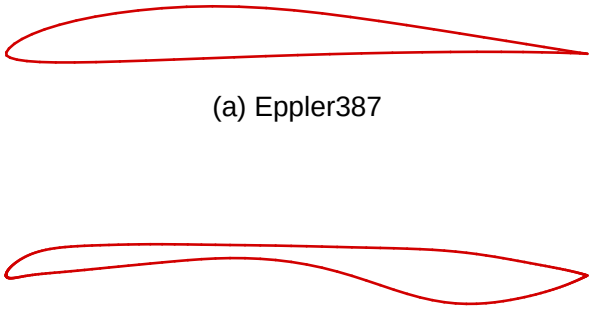

(a) Eppler387

(b) SPLRM

Figure 6 Shape of Eppler 387 and SPLRM airfoils

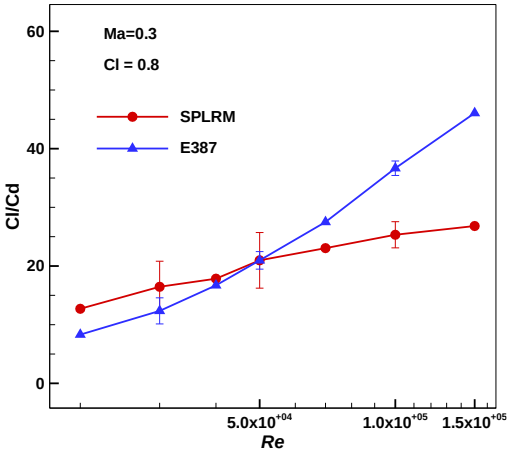

Figure 7 Comparison of lift-to-drag ratio between Eppler 387 and SPLRM airfoils

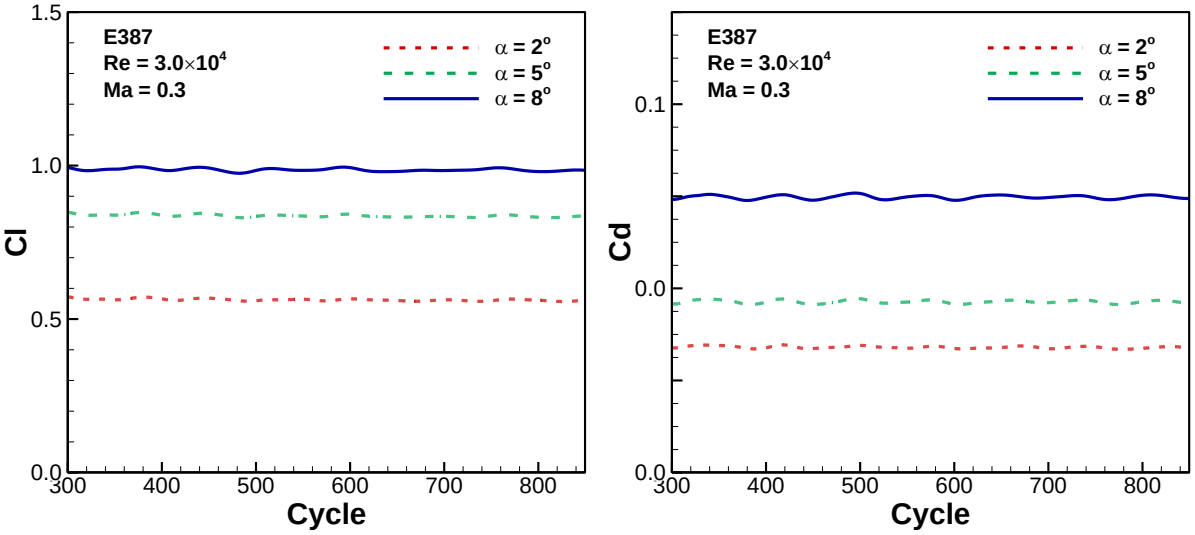

(a) lift coefficient (b) drag coefficient

Figure 8 Convergence of unsteady force of E387 airfoils

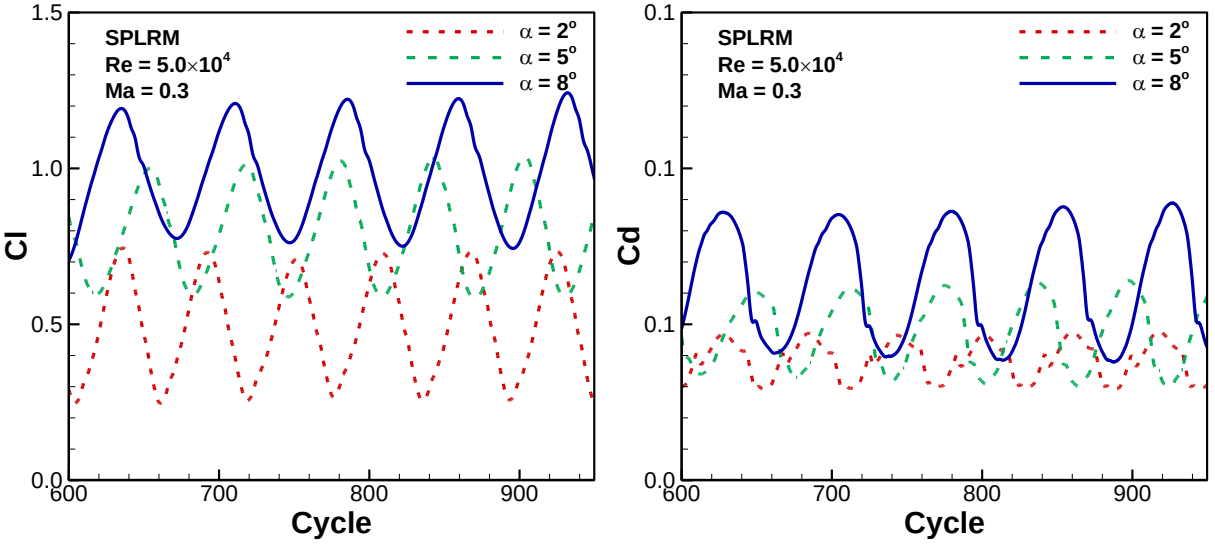

(a) lift coefficient (b) drag coefficient

Figure 9 Convergence of unsteady force of SPLRM airfoils

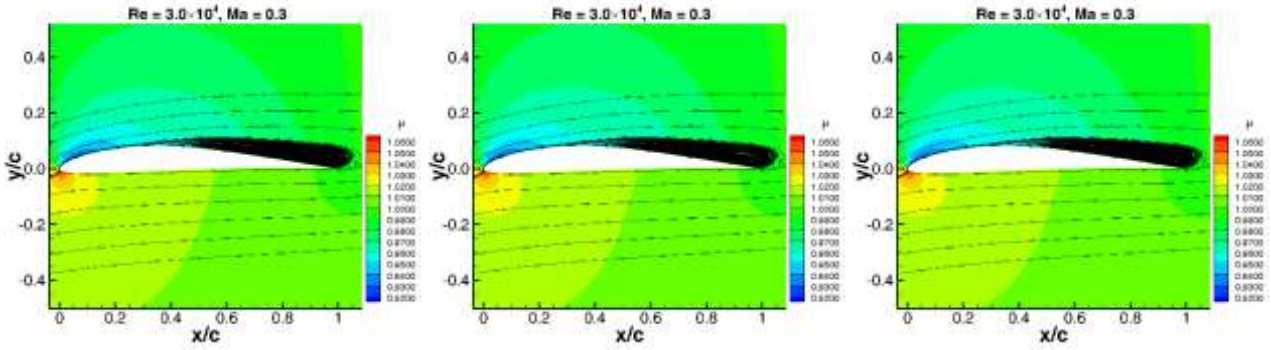

Figure 10 Unsteady laminar separation bubble of E387 airfoils (c_l = 0.8)

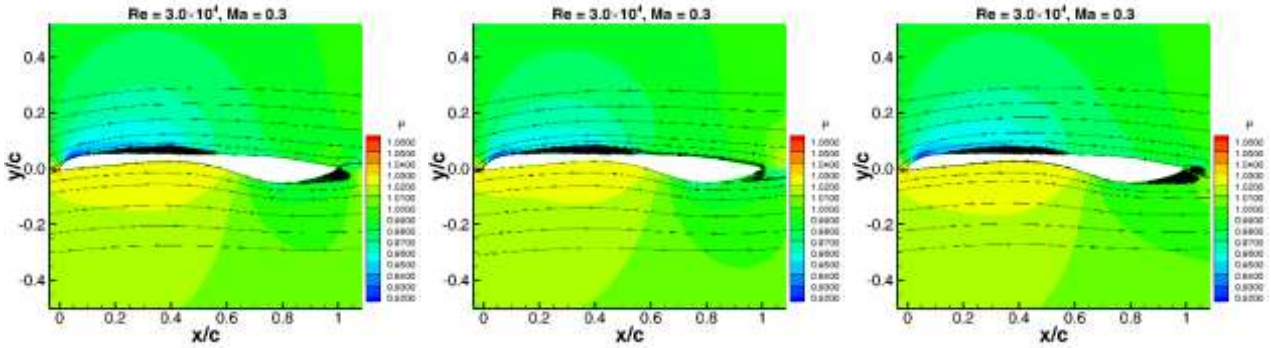

Figure 11 Unsteady laminar separation bubble of SPLRM airfoils (c_l = 0.8)

4. Unsteady Design of Airfoil

According to the analysis of section 3, the aim of this paper is to reduce the thickness of laminar separation bubble on the upper surface of airfoil to achieve lower drag and higher lift-to-drag ratio, and to reduce the separation on the lower surface of airfoil to reduce the unsteady characteristics. Therefore, two objectives are introduced: time-averaged value and amplitudes of unsteady drag. The mathematical model of optimization for single-point design can be expressed as follows:

$$\begin{aligned} \min \quad & \omega_1 \frac{\bar{C}_d}{\bar{C}_{d,baseline}} + \omega_2 \frac{A_m}{A_{m,baseline}} \\ s.t. \quad & (1)\ \bar{C}_l \geq \bar{C}_{l,baseline} \\ & (2)\ (t/c) \geq (t/c)_{baseline} \end{aligned} \tag{1}$$

where, ω_1 and ω_2 are weighted coefficients of the two objectives, and $\omega_1 + \omega_2 = 1$. $\bar{C}_d$ and $\bar{C}_l$ denotes

time-averaged drag and lift, respectively. A_m denotes amplitudes. *t/c* is the thickness of airfoil.

The mathematical model of optimization for single-point design can be expressed as follows:

$$\begin{aligned} \min \quad & \omega_5\left(\omega_1\frac{C_{d1}}{C_{d1,baseline}}+\omega_2\frac{A_{m1}}{A_{m1,baseline}}\right)+\omega_6\left(\omega_3\frac{C_{d2}}{C_{d2,baseline}}+\omega_4\frac{A_{m2}}{A_{m2,baseline}}\right) \\ s.t. \quad & (1)\ C_l \geq C_{l,baseline} \\ & (2)\ (t/c) \geq (t/c)_{baseline} \end{aligned} \tag{2}$$

where, $\omega_1 + \omega_2=1$, $\omega_3 + \omega_4=1$, $\omega_5 + \omega_6=1$. It should be pointed out that the moment of airfoil is not considered because there is no strict requirement for moment in the design of propeller blade.

Simulation of unsteady flow is very time-consuming and it is unacceptable to use URANS in optimal design. Therefore, an efficient optimizer based on Kriging surrogate model, named "SurroOpt"[9]-[13] is used in this paper. The surrogate-based optimization method is proven to be efficient and robust. As shown in Figure 12, the Latin Hypercube Sampling (LHS) method[12] was used to generate initial sample points in the design space, which was called design of experiment (DoE). In addition, a parallel infilling strategy[10], including expected improvement (EI)[14], minimizing surrogate prediction (MSP)[15], maximizing the probability of improvement function (PI)[16], maximizing the mean squared error (MSE)[16] and Minimizing the lower confidence bounding (LCB)[17], is chosen to add new sample points simultaneously.

Class function/Shape function Transformation (CST)[18] method is used as parameterization method of Airfoil shape. The order of the Bernstein polynomial is 8 and 18 variables are optimized.

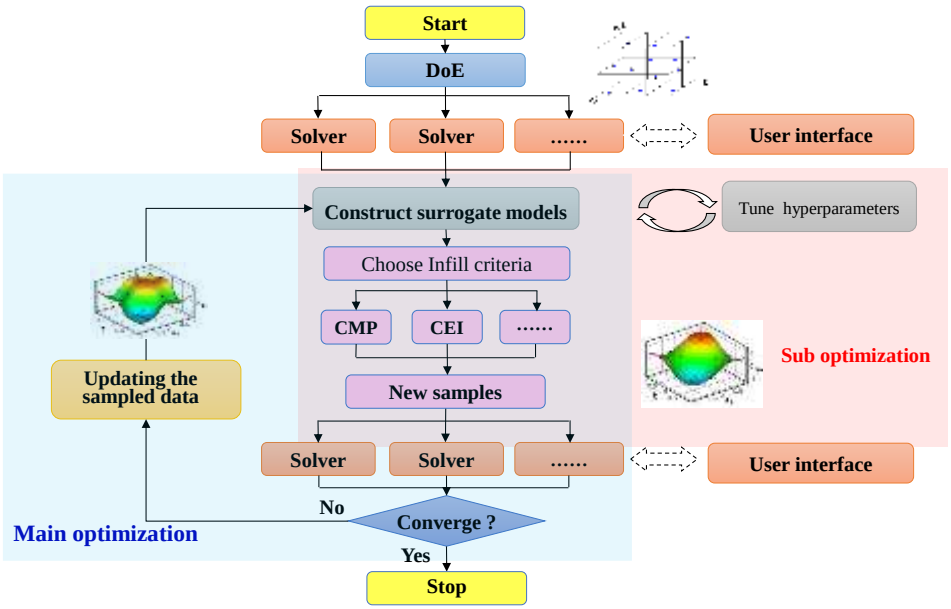

Figure 12 Framework of the efficient surrogate-based optimizer: SurroOpt

5. Results and Discussion

The baseline used for optimization is SPLRM spoon shaped airfoil, developed by Zhang et al[3]. Two cases are investigated, including 1) single-point optimization with the flow condition of Ma=0.3, Re=50,000, α=4°; 2) two- point optimization with the flow conditions of Ma=0.3, Re=50,000, α=4°; and Ma=0.3, Re=100,000, α=3°.

5.1 Single-Point Design Optimization

For this optimization design, the weighted coefficients ω_1 and ω_2 are 0.5 and 0.5. Figure 13 shows the convergence history of optimization design. Compared with the baseline airfoil, the objective function value of the optimized airfoil is reduced by 60%. Figure 14 shows the comparison of baseline and optimum airfoil. Compared with baseline airfoil, both the maximum camber and maximum thickness of

the optimum airfoil are increased, and the location of maximum thickness moved forward obviously. Figure 15 demonstrates that the optimum airfoil has higher time-averaged lift coefficient and lower time-averaged drag coefficient. Moreover, the unsteady amplitudes of lift and drag are significantly reduced. Figure 16 shows that the lift and drag characteristics are improved in a wide range of angles of attack, especially the unsteady amplitudes are significantly reduced. The absolute of moment coefficient increases, but is still acceptable in the design of propeller. The unsteady aerodynamic force of the baseline airfoil is mainly caused by the unsteady separated flow at the trailing edge on lower surface, as shown in Figure 17. The optimum airfoil only has laminar separation bubble on the upper surface, but no separation flow on the trailing edge, as shown in Figure 18. Therefore, the unsteady effect of the optimum airfoil is obviously weakened.

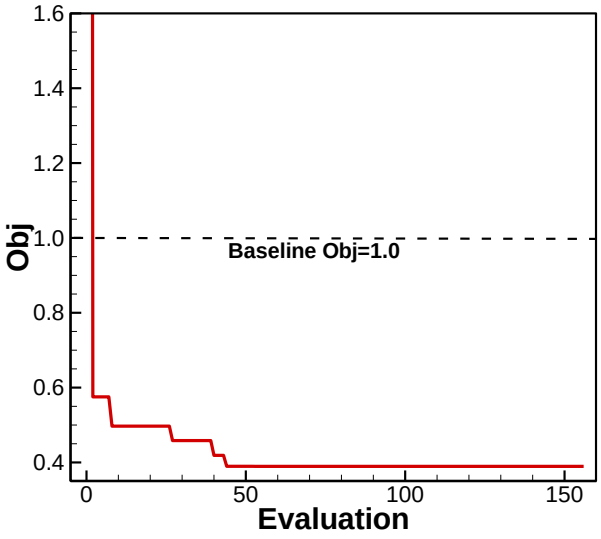

Figure 13 Convergence history of optimization design (single-point design)

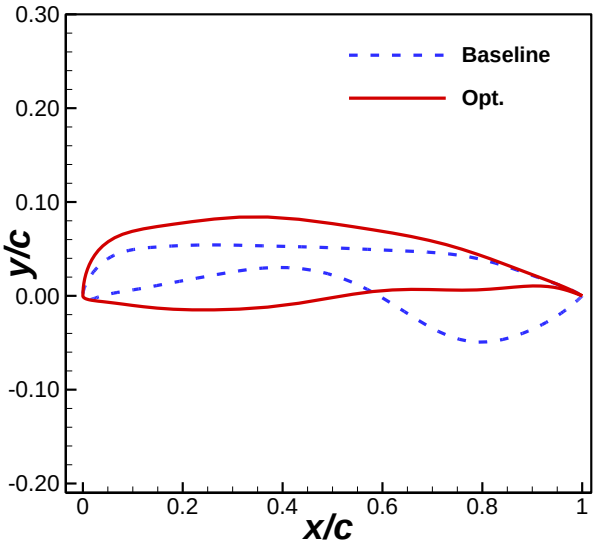

Figure 14 Comparison of baseline and optimum airfoil (single-point design)

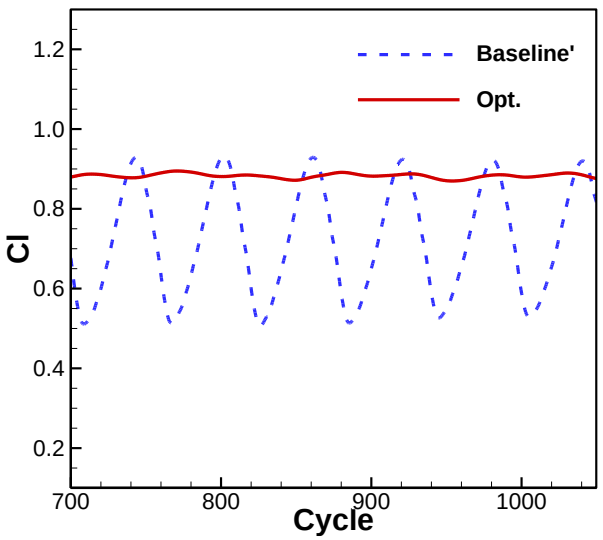

(a) lift coefficient

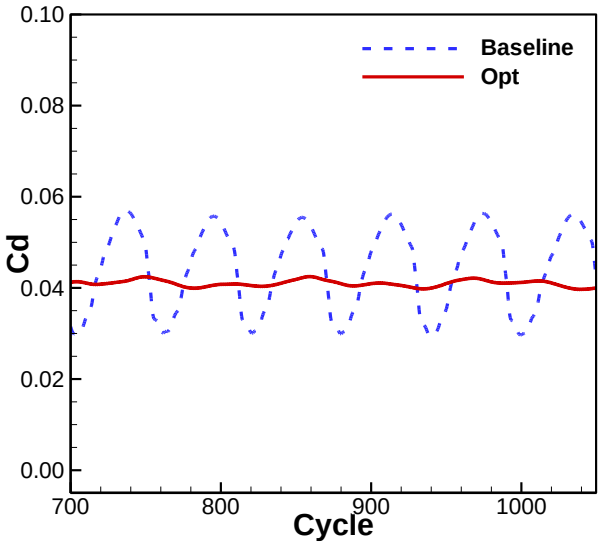

(b) drag coefficient

Figure 15 Comparison of lift coefficient and drag coefficient at the design point (Ma=0.3, Re=50,000, α=4°) between baseline and optimum airfoils (single-point design)

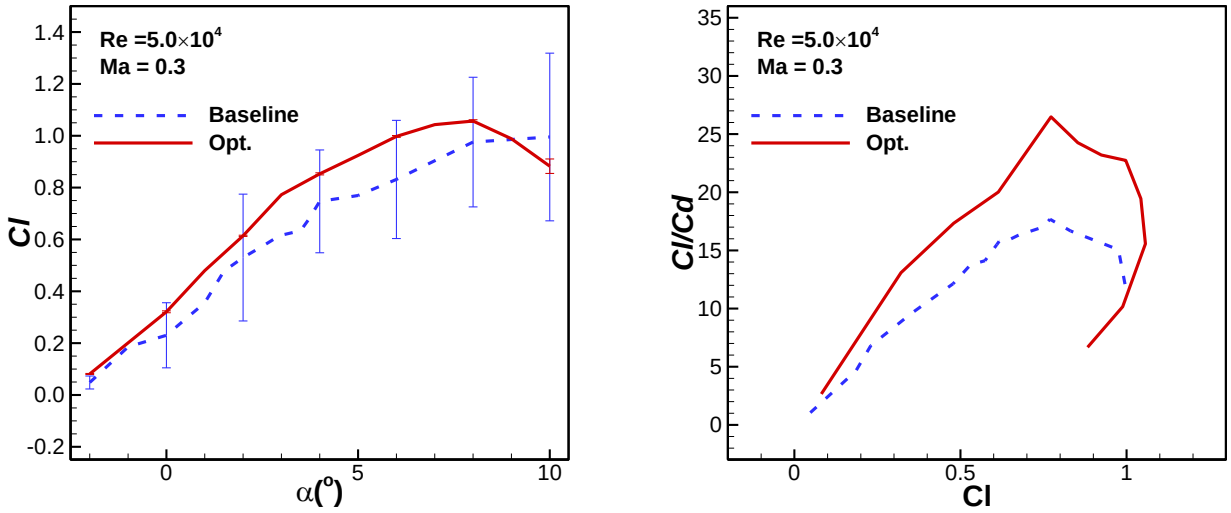

(a) lift

(b) lift-to-drag ratio

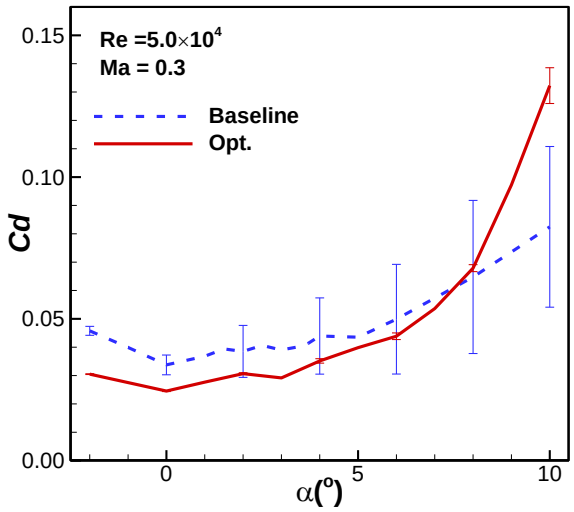

(c) drag

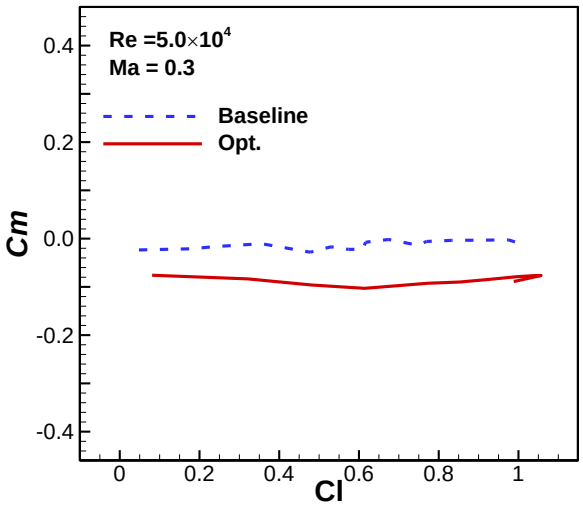

(d) moment

Figure 16 Comparison of aerodynamic force between baseline and optimum airfoils (single-point design)

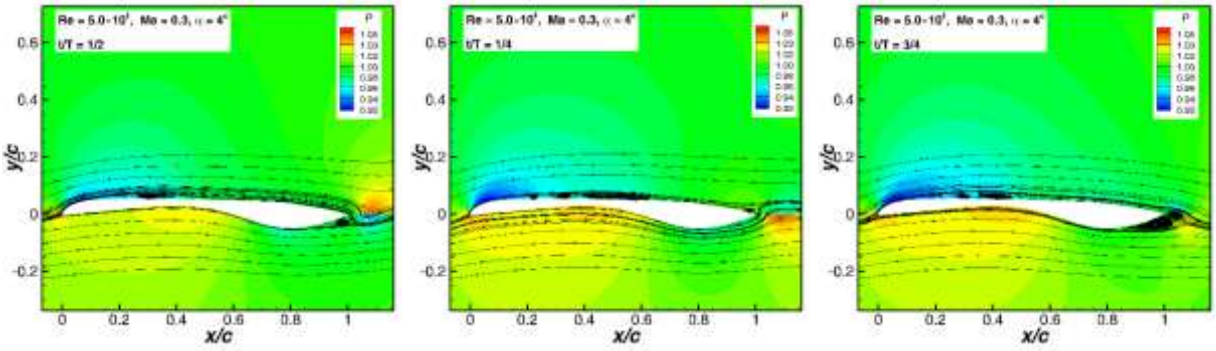

Figure 17 Pressure contour and laminar separation bubble at typical time (baseline airfoil)

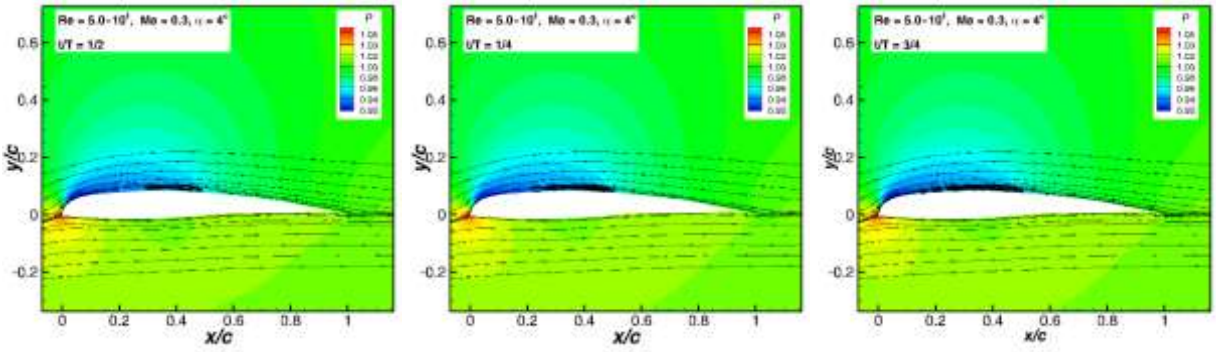

Figure 18 Pressure contour and laminar separation bubble at typical time (optimum airfoil)

5.2 Two-Point Design Optimization

The second case is a two-point design optimization. All of the weighted coefficients, ω_1 to ω_6, are fixed to 0.5. Figure 19 shows the convergence history of optimization design. Figure 20 shows the Comparison of baseline and optimum airfoil. Figure 21 and Figure 22 show that for both the two design points, the time-averaged lift coefficients are increased and the time-averaged drag coefficient are reduced. The improvement is more obvious at design point of Ma=0.3, Re=10,000, α=3°. Meanwhile, the amplitudes of lift and drag are significantly reduced. In addition, the comprehensive aerodynamic performance has been greatly improved, as shown in Figure 23 and Figure 24.

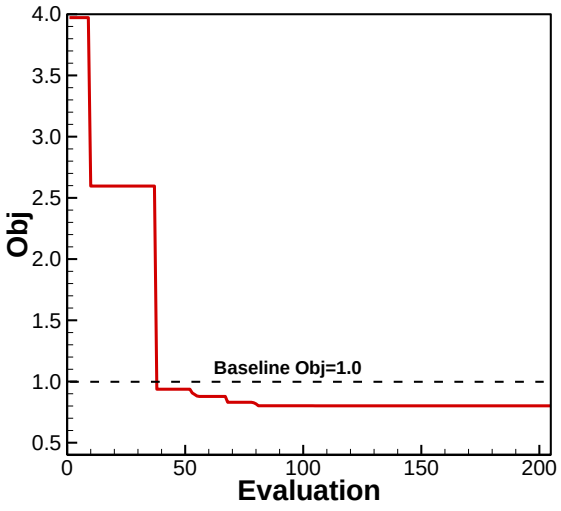

Figure 19 Convergence history of optimization design (two-point design)

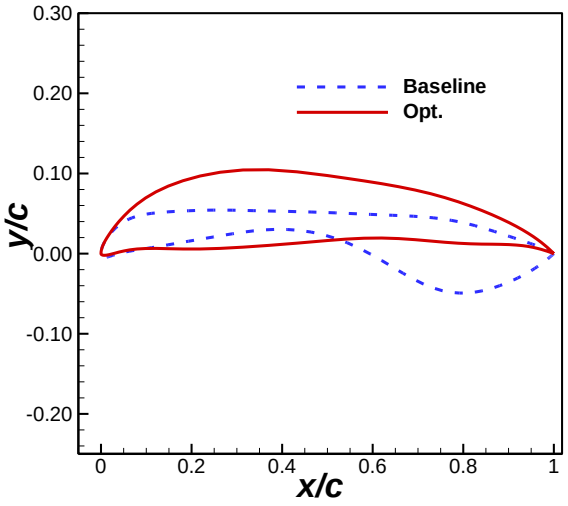

Figure 20 Comparison of baseline and optimum airfoil (two-point design)

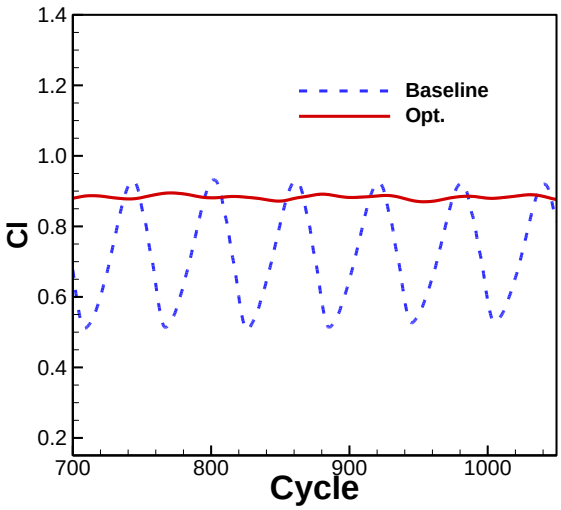

(a) lift coefficient

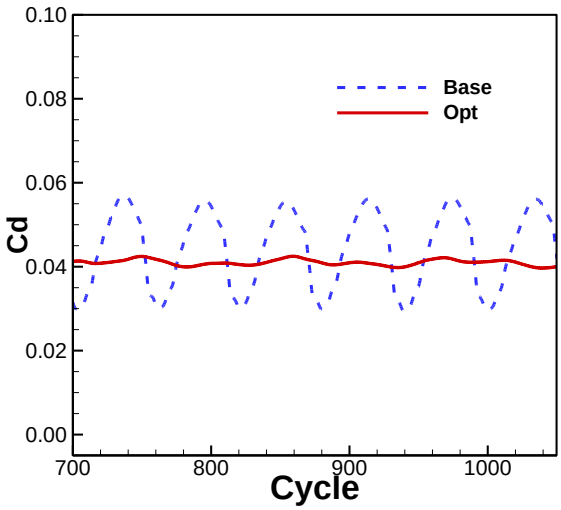

(b) drag coefficient

Figure 21 Comparison of lift coefficient and drag coefficient at the design point (Ma=0.3, Re=50,000, α=4°) between baseline and optimum airfoils (two-point design)

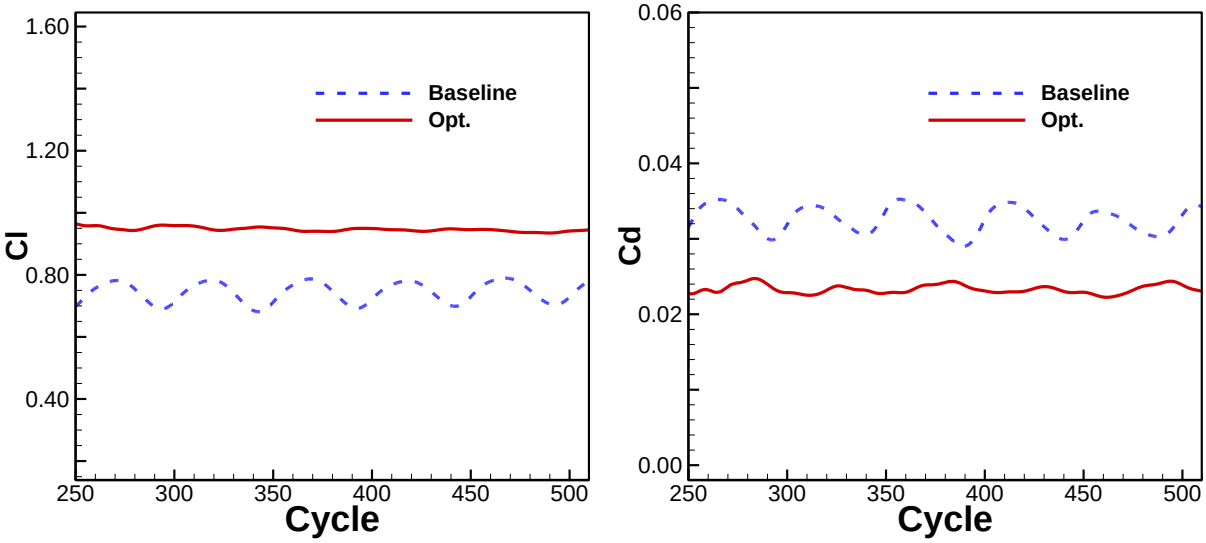

(a) lift coefficient (b) drag coefficient

Figure 22 Comparison of lift coefficient and drag coefficient at the design point (Ma=0.3, Re=10,000, α=3°) between baseline and optimum airfoils (two-point design)

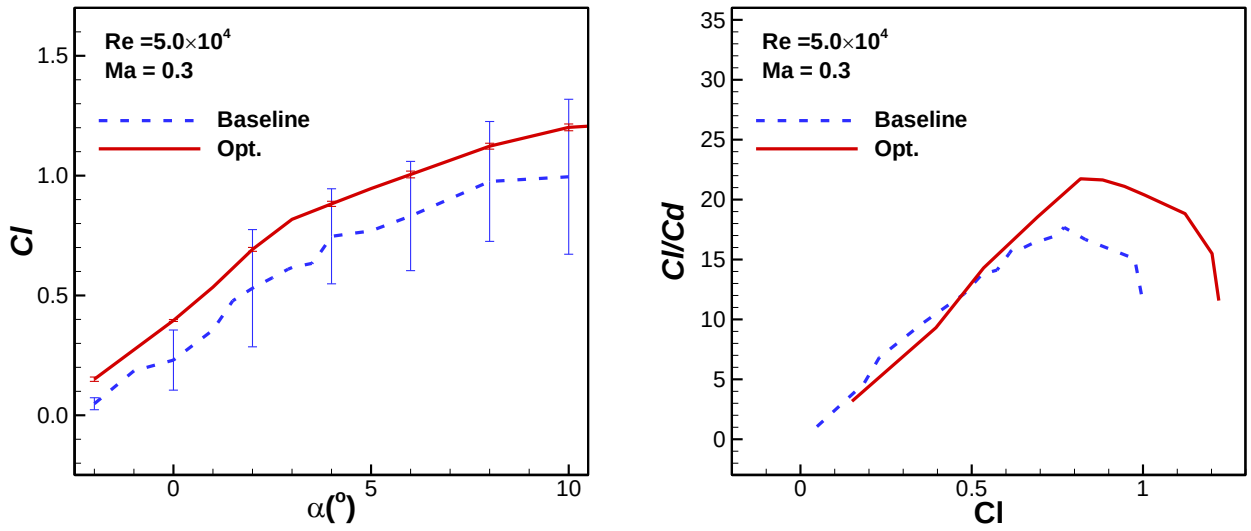

(a) lift (b) lift-to-drag

Figure 23 Comparison of aerodynamic performance between baseline and optimum airfoils (two-point design, Ma=0.3, Re=50,000)

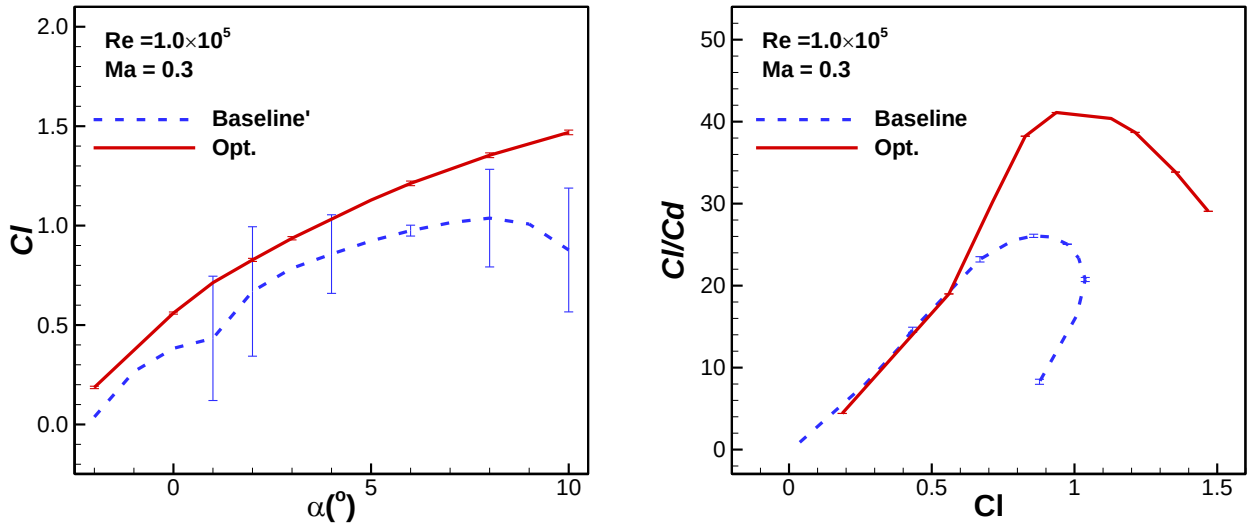

(a) lift (b) lift-to-drag

Figure 24 Comparison of aerodynamic performance between baseline and optimum airfoils (two-point design, Ma=0.3, Re=10,000)

6. Conclusions

(1) The special shaped airfoil may have higher lift-to-drag ratio, but instable long laminar separation bubble leads to aerodynamic force fluctuate greatly.

(2) An unsteady aerodynamic design method is developed, with time-averaged value and fluctuation of drag as two optimal objectives.

(3) The results of single-point and two-point optimization design demonstrate that both the time-averaged drag and fluctuation are reduced significantly.

7. Contact Author Email Address

mailto: wpsong@nwpu.edu.cn

8. Copyright Statement

References

[1] Srinath D N, Mittal S. Optimal Airfoil Shapes for Low Reynolds Number Flows. *International Journal for Numerical Methods in Fluids*, Vol. 61, No. 4, pp 355-381, 2010.

[2] Srinath D N, Mittal S. Optimal Aerodynamic Design of Airfoils in Unsteady Viscous Flows. *Computer Methods in Applied Mechanics & Engineering*, Vol. 199, No. 29-32, pp 1976-1991, 2010.

[3] Zhang S L, Yang X D, Song B F, Song W P. Aerodynamic Design of a Novel Low-Reynolds-Number Airfoil for Near Space Propellers. *Proceedings of 2015 Asian-Pacific Conference on Aerospace Technology and Science*, Jeju Island, Korea, 20-23 May, 2015.

[4] McGhee R J, Walker B S, Millard B F. Experimental Results for the Eppler387 Airfoil at Low Reynolds Numbers in the Langley Low-turbulence Pressure Tunnel. NASA TM-4062, 1988.

[5] Jameson A, Schmidt W, and Turkel E, Numerical Solutions of the Euler Equations by a Finite Volume Method Using Runge-Kutta Time Stepping Schemes. AIAA Paper 1981-1259, 1981

[6] Han Z H. Efficient Method for Simulation of Viscous Flows past Helicopter Rotors and Active Flow Control. D. Dissertation, Northwestern Polytechnical University, 2007.

[7] Menter F R. Two-Equation Eddy-Viscosity Turbulence Models for Engineering Applications. *AIAA Journal*, Vol. 32, No. 8, pp 1598-1605, 1994.

[8] Menter F R, Langtry R B, Likki S R, et al. A Correlation-Based Transition Model Using Local Variables-Part I: Model Formulation. *Journal of Turbomachinery*, Vol. 128, No. 3, pp 413-422, 2006.

[9] Han Z H. SURROOPT: A Generic Surrogate-Based Optimization Code for Aerodynamic and Multidisciplinary Design. *In Proceedings of the 30th Congress of the International Council of the Aeronautical Sciences*, DCC, Daejeon, Korea, 25–30 September, 2016.

[10] Liu J, Song W P, Han Z H, Zhang Y. Efficient Aerodynamic Shape Optimization of Transonic Wings Using a Parallel Infilling Strategy and Surrogate Models. *Structural and Multidisciplinary Optimization*. Vol. 55, pp 925–943, 2017.

[11] Han Z H, Xu, C Z, Zhang L, Zhang Y, Zhang K S, Song W P. Efficient Aerodynamic Shape Optimization Using Variable-Fidelity Surrogate Models and Multilevel Computational Grids. *Chinese Journal of Aeronautics*, Vol. 33, No. 1, pp 31-47, 2020.

[12] Han Z H, Chen J, Zhang K S, Xu Z M, Zhu Z, Song W P. Aerodynamic Shape Optimization of Natural-Laminar-Flow Wing Using Surrogate-Based Approach. *AIAA Journal*. Vol. 56, No. 7, pp 2579-2593, 2018.

[13] Liu F, Han Z H, Zhang Y, Song K, Song W P, Gui F, Tang J B. Surrogate-Based Aerodynamic Shape Optimization of Hypersonic Flows Considering Transonic Performance, *Aerospace Science and Technology*, Vol. 93, pp 105345, 2019.

[14] Jones D R, Schonlau M, Welch W J. Efficient Global Optimization of Expensive Black-Box Functions. *Journal of Global Optimization*. Vol. 13, pp 455-492, 1998.

[15] Booker A J, Dennis J E, Frank P D, Serafini D B, Torczon V, Trosset M W. A Rigorous Framework for Optimization of Expensive Functions by Surrogates. *Structural Optimization*, Vol. 17, No. 1, pp 1-13, 1998.

[16] Forrester A I J, Keane A J. Recent Advances in Surrogate-Based Optimization. *Progress in Aerospace*

Sciences, Vol. 45, No. 1-3, pp 50-79, 2009.

[17]Laurenceau J, Meaux M, Montagnac M, Sagaut P. Comparison of Gradient-Based and Gradient-Enhanced Response-Surface-Based Optimizers. *AIAA Journal*, Vol. 48, No. 5, pp 981-994, 2010.

[18]Kulfan B M. A Universal Parametric Geometry Representation Method – “CST”, AIAA 2007-62, 2007.